RalA controls glucose homeostasis by regulating glucose uptake in brown fat

Yuliya Skorobogatko[a,b], Morgan Dragan[a], Claudia Cordon[b], Shannon M. Reilly[a,b], Chao-Wei Hung[a], Wenmin Xia[a,c], Peng Zhao[a,b], Martina Wallace[d], Denise E. Lackey[a], Xiao-Wei Chen (陈晓伟)[b], Olivia Osborn[a], Juliane G. Bogner-Strauss[c], Dan Theodorescu[e], Christian M. Metallo[d], Jerrold M. Olefsky[a], and Alan R. Saltiel[a,b,1]

[a]Department of Medicine, University of California, San Diego School of Medicine, La Jolla, CA 92093; [b]Life Sciences Institute, University of Michigan, Ann Arbor, MI 48109; [c]Institute of Biochemistry, Graz University of Technology, 8010 Graz, Austria; [d]Jacobs School of Engineering, University of California, San Diego, La Jolla, CA 92093; and [e]Department of Surgery, University of Colorado, Aurora, CO 80045

Edited by Jeffrey E. Pessin, Albert Einstein College of Medicine, Bronx, New York, and accepted by Editorial Board Member David J. Mangelsdorf May 25, 2018 (received for review January 22, 2018)

Insulin increases glucose uptake into adipose tissue and muscle by increasing trafficking of the glucose transporter Glut4. In cultured adipocytes, the exocytosis of Glut4 relies on activation of the small G protein RalA by insulin, via inhibition of its GTPase activating complex RalGAP. Here, we evaluate the role of RalA in glucose uptake in vivo with specific chemical inhibitors and by generation of mice with adipocyte-specific knockout of RalGAPB. RalA was profoundly activated in brown adipose tissue after feeding, and its inhibition prevented Glut4 exocytosis. RalGAPB knockout mice with diet-induced obesity were protected from the development of metabolic disease due to increased glucose uptake into brown fat. Thus, RalA plays a crucial role in glucose transport in adipose tissue in vivo.

RalGAP | GTPase | Ral inhibitors | Glut4 | insulin

Although adipose tissue accounts for only 10 to 15% of insulin-stimulated glucose uptake, it serves as a primary site for energy storage and coordinates systemic energy metabolism (1). Exceeding the storage capacity of adipocytes leads to ectopic lipid deposition and subsequent metabolic dysregulation in muscle and liver. Moreover, adipocytes serve as a cellular "rheostat" that senses whole-body energy status and responds by secreting hormones, cytokines, chemokines, and adipokines that regulate metabolism in muscle, liver, and brain (2). Glucose transport into adipocytes thus plays an important role in modulating energy metabolism. In this regard, genetic manipulations that increase glucose uptake into fat produce systemic improvements in glycemic control, reduced ectopic lipid deposition, and reduced inflammation (3, 4), suggesting a key role for adipose tissue in global regulation of metabolism.

Insulin-stimulated glucose uptake in fat and muscle is mediated by the major facilitative glucose transporter, Glut4. Insulin increases glucose uptake by controlling the trafficking of Glut4 to the plasma membrane via regulation of a series of small G proteins (5). We had implicated RalA in the regulation of Glut4 exocytosis in 3T3-L1 adipocytes by insulin. RalA associates with Glut4 storage vesicles (GSVs) and, once activated by insulin, binds to the tethering exocyst complex, thus positioning GSVs in close proximity to plasma membrane for efficient Glut4 docking and fusion (6). RalA activity is regulated by the Ral GTPase activating protein (GAP) complex, which maintains RalA in its inactive GDP-bound state under basal conditions. The complex consists of RalGAPB, a scaffolding protein that is required to stabilize the complex, and RalGAPA2 (the RalGAPA isoform expressed in adipocytes), a protein with RalGAP activity. The RalGAP complex bears some similarity to the Rheb GAP tuberous sclerosis complex, but is exquisitely specific for Ral (7). In response to insulin, RalGAPA2 is phosphorylated by AKT, subsequently interacts with 14-3-3, and is thus sequestered away from RalA, producing RalA activation (8). Activated RalA associates with Glut4 vesicles and, in response to insulin, binds to Exo84 and Sec5, subunits of the exocyst complex, which tethers the GSV at the plasma membrane for docking and fusion. Knockdown of RalA in 3T3-L1 adipocytes inhibits cell surface Glut4 exposure and glucose uptake (6). Conversely, knockdown of RalGAP subunits increases RalA activity, leading to potentiation of insulin-stimulated Glut4 exocytosis and increased glucose uptake (7).

To address the contribution of RalA and its GAP complex to Glut4 exocytosis and glucose metabolism in vivo, we administered specific Ral inhibitors to mice, and also generated mice with adipocyte-specific knockout of RalGAPB, which dramatically increased RalA activity. Here, we report that Ral inhibitors reduce glucose uptake into brown adipose tissue (BAT) and, in the process, elevate glucose levels in serum. Moreover, RalGAPB knockout mice exhibit increased glucose disposal in BAT, which leads to increased adiposity, lower fasting blood glucose and insulin levels, and improved whole-body glucose handling. These data suggest that the RalA pathway is a crucial regulator of glucose metabolism in vivo.

Results

RalA Inhibitors Dramatically Reduce Glut4 Exocytosis and Insulin-Stimulated Glucose Uptake in 3T3-L1 Adipocytes. Previous studies implicated a crucial role for RalA in the regulation of Glut4 recycling and insulin-stimulated glucose uptake in 3T3-L1 adipocytes (6–9). To test the role of RalA in glucose uptake in vivo, we employed recently developed allosteric Ral inhibitors. These compounds bind to and stabilize Ral in its inactive, GDP-bound state and are highly selective toward Ral (*SI Appendix*, Fig. S1*A*) (10). We first tested the effect of the Ral inhibitors on glucose

Significance

The primary event in diabetes pathogenesis is the development of insulin resistance. Insulin is elevated during feeding and maintains blood glucose levels within a physiological range, largely by increasing glucose uptake in muscle and fat. Our laboratory has identified two components of insulin signaling, the protein RalA and its GAP complex RalGAP, which regulate glucose uptake by fat cells. Using genetic approaches and pharmacological inhibitors, we describe how these proteins influence glucose metabolism in mice. We discovered that RalA is essential for efficient insulin-stimulated glucose uptake in fat, while RalA activation via deletion of RalGAP dramatically increases glucose uptake into brown fat and improves glucose handling in mice (hence, protecting them from developing diabetes).

Author contributions: Y.S., J.G.B.-S., C.M.M., J.M.O., and A.R.S. designed research; Y.S., M.D., C.C., S.M.R., C.-W.H., W.X., P.Z., M.W., D.E.L., X.-W.C., O.O., and D.T. contributed new reagents/analytic tools; Y.S., M.D., C.C., C.-W.H., and M.W. analyzed data; and Y.S. and A.R.S. wrote the paper.

The authors declare no conflict of interest.

This article is a PNAS Direct Submission. J.E.P. is a guest editor invited by the Editorial Board.

See Commentary on page 7651.

[1]To whom correspondence should be addressed. Email: asaltiel@ucsd.edu.

This article contains supporting information online at www.pnas.org/lookup/suppl/doi:10.1073/pnas.1801050115/-/DCSupplemental.

Published online June 18, 2018.

uptake in 3T3-L1 adipocytes, in which RalA knockdown inhibits Glut4 exocytosis and insulin-stimulated glucose uptake (6). Pretreatment of adipocytes with the structurally distinct Ral inhibitors BQU57 and RBC8 produced a statistically significant inhibition of insulin-stimulated glucose uptake (Fig. 1*A* and *SI Appendix*, Fig. S1*B*). BQU57 inhibited insulin-stimulated glucose uptake in a dose-dependent manner (Fig. 1*B*) but did not affect AKT phosphorylation in response to insulin or protein levels of the glucose transporters Glut1 and Glut4, implying an effect on Glut4 trafficking (*SI Appendix*, Fig. S1 *C–F*). Accordingly, treatment of cells with BQU57 reduced the plasma membrane localization of endogenous Glut4 as well as a 7Myc-Glut4-EGFP reporter in response to insulin (Fig. 1 *C* and *D* and *SI Appendix*, Fig. S2 *A–C*).

RalA Inhibition Alters Glut4 Vesicle Dynamics by Decreasing Tethering. We have previously shown that RalA associates with Glut4 vesicles when activated by insulin. RalA also serves as a cargo receptor for the myosin motor protein Myo1c and is required for Glut4 vesicle trafficking along actin filaments. Upon translocation of Glut4 vesicles, activated RalA mediates Glut4 vesicle tethering via interaction with its effectors Sec5 and Exo84, subunits of the exocyst complex (6).

We explored the trafficking of Glut4 by total internal reflection fluorescence (TIRF) microscopy (11). Treatment of 3T3-L1 adipocytes with insulin dramatically increased the intensity of Glut4-EGFP puncta in the TIRF zone within 3 min, while BQU57 prevented translocation of Glut4-EGFP into the TIRF zone (Fig. 1 *F* and *G* and *SI Appendix*, Fig. S2*D*). To better characterize the effect BQU57 on insulin-induced Glut4 translocation, we measured the diffusion coefficient of Glut4. At the basal state, the distribution of Glut4 diffusion coefficient exhibits one broad peak (3×10^{-15} to 1×10^{-14} m^2/s) and one narrow peak (3×10^{-14} to 5×10^{-14} m^2/s), whereas in the insulin-stimulated state, a third peak with low diffusion coefficient is observed ($<1 \times 10^{-15}$ m^2/s) (*SI Appendix*, Fig. S3*A*). Low diffusion coefficient indicates vesicles preparing for fusion (12, 13). Due to the presence of three distinct peaks in the insulin-stimulated state, we classified Glut4 vesicles into three groups based on their diffusion coefficient: slow ($<1 \times 10^{-15}$ m^2/s), medium (1×10^{-15} to 1×10^{-14} m^2/s), and fast (1×10^{-15} to 1×10^{-13} m^2/s). Pretreatment with BQU57 did not change the number of peaks in the distribution curve; however, cells pretreated with BQU57 displayed only a threefold increase in vesicles that are categorized as slow, whereas DMSO-treated cells displayed a 12.5-fold increase in slow vesicles (*SI Appendix*, Fig. S2 *A* and *B*). This result indicates that pretreatment with BQU57 impairs insulin-induced Glut4 vesicle tethering/docking.

RalA Inhibition Attenuates Insulin-Stimulated Glucose Uptake into BAT. To test whether RalA regulates glucose uptake in vivo, we administered RBC8 via i.p. injection to ad libitum-fed mice. The compound increased blood glucose and insulin levels, reaching a maximal effect 40 min after administration (Fig. 1 *H* and *I*), indicative of inhibition of peripheral glucose disposal. Next, we measured in vivo glucose uptake in individual tissues 40 min after RBC8 injection. The radioactive glucose tracer disappeared from plasma of RBC8-treated mice more slowly than was observed in DMSO-treated controls (*SI Appendix*, Fig. S4*A*). Glucose uptake into BAT was reduced by 38%, while glucose uptake into other insulin-responsive tissues and brain was not affected (RBC8 does not cross the blood brain barrier) (Fig. 1*J*). RalA was activated by feeding in BAT, and RBC8 administration significantly reduced RalA activity in BAT in vivo (Fig. 1*K*) but

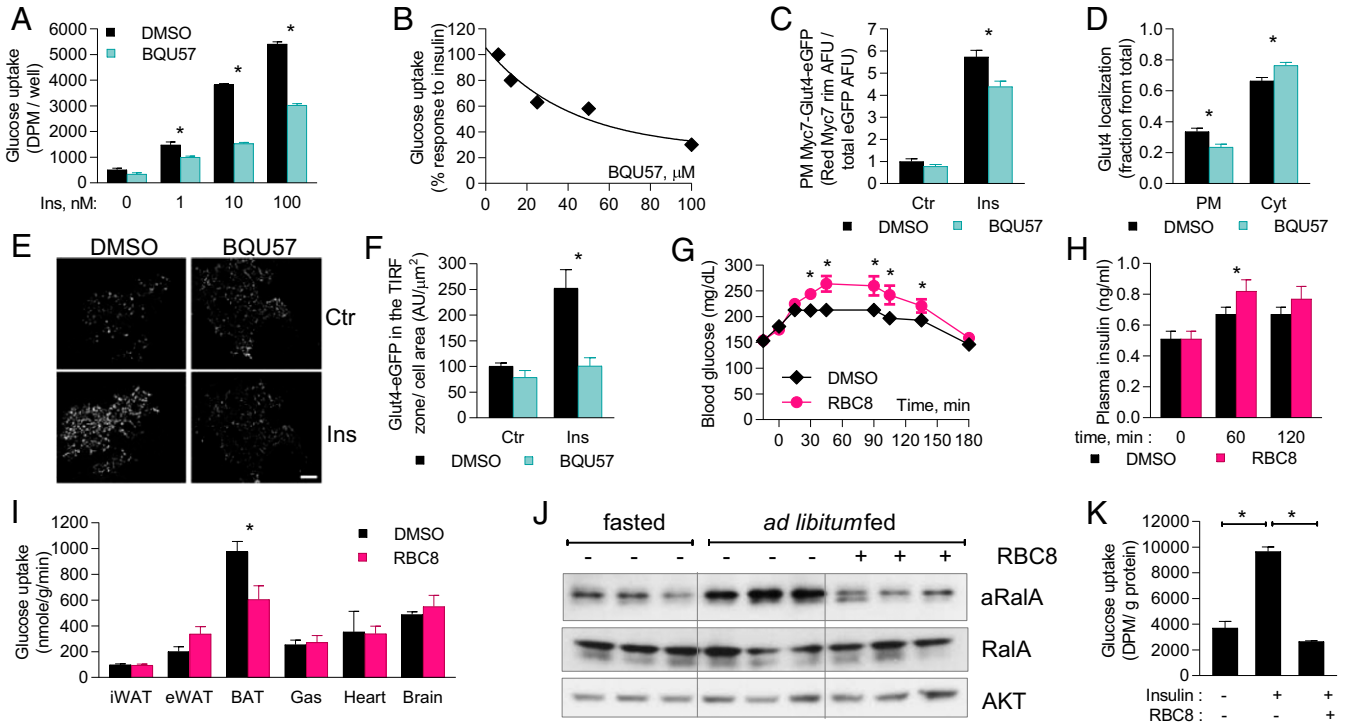

Fig. 1. Ral inhibitors reduce glucose uptake and plasma membrane localization of Glut4. (*A–G*) 3T3-L1 adipocytes were pretreated with 100 μM BQU57 for 1 h and stimulated with 10 nM insulin for 30 min, unless indicated otherwise. (*A* and *B*) Glucose uptake in 3T3-L1 adipocytes treated with (*A*) 50 μM BQU57 and various concentrations of insulin and (*B*) dilutions of BQU57 and 10 nM insulin; four replicates for each condition. (*C*) Quantitation of Myc7-Glut4-EGFP localization in 3T3-L1 adipocytes; 22 cells per group. (*D*) Quantitation of endogenous Glut4 localization; 22 control and 25 BQU57-treated cells. (*E* and *F*) TIRF imaging of Myc7-Glyt4-EGFP in 3T3-L1 adipocytes 3 min after insulin administration (*E*) and its quantitation (*F*); five cells in each condition. (*G–J*) Ad libitum-fed lean mice were i.p. injected with 50 mg/kg RBC8. (*G* and *H*) Blood glucose (*G*) and insulin (*H*) levels; 11 mice per group. (*I*) 2-Deoxy-D-glucose-phosphate in tissues 40 min after RBC8 administration; eight mice per group. (*J*) WB of BAT lysates at 40-min time point. (*K*) 2-Deoxy-D-glucose uptake in primary brown adipocytes. The data are presented as mean ± SEM; $^*P < 0.05$. aRalA, active RalA; Ctr, control; Cyt, cytosolic; PM, plasma membrane.

had no effect on RalA activity in white adipose tissue (WAT) (*SI Appendix*, Fig. S4 *B* and *C*). In addition, RBC8 completely inhibited insulin-stimulated glucose uptake in brown adipocytes that were differentiated in vitro from BAT-derived preadipocytes (Fig. 1*K* and *SI Appendix*, Fig. S4*D*). RBC8 also inhibited lipogenesis in primary adipocytes differentiated from inguinal WAT (iWAT)-derived preadipocytes under conditions in which glucose transport is rate limiting (*SI Appendix*, Fig. S4*E*). Together, these findings indicate that RalA activation is required for insulin-stimulated glucose uptake in both brown and white adipocytes but that in vivo administration of Ral inhibitors only blocks RalA activity in BAT.

Adipose-Specific Knockout of RalGAPB Activates RalA. We have previously established that the RalGAP complex maintains RalA in the inactive state in 3T3-L1 adipocytes. siRNA-mediated knockdown of RalGAP subunits activates RalA and increases glucose uptake in 3T3-L1 adipocytes (7). To test the role of RalA in glucose uptake in adipose tissue in vivo, we generated C57BL/6J mice, with exon 3 of the *Ralgapb* gene surrounded by flox sites, and bred them with AdipoQ-Cre mice. Crossing these mice resulted in adipocyte-specific RalGAPB knockout (ARGKO) mice, with efficient deletion of RalGAPB in all adipose tissue depots, although there was residual protein, presumably due to the presence of nonadipocytes. Interestingly, targeted RalGAPB deletion produced robust activation of RalA in all adipose tissues (Fig. 2*A*), confirming that the RalGAP complex keeps RalA in the GDP-bound state in adipose tissue in vivo. Importantly, the levels of GTP-bound RalA in ARGKO mice were not reduced by RBC8 treatment, indicating that RalA does not cycle through the GDP-bound state in the absense of RalGAPB and that it is constitutively activated and insensitive to inhibitors that interact with and stabilize RalA in its GDP-bound, inactive state (*SI Appendix*, Fig. S4 *B*, *C*, *F*, and *G*).

Adipose-Specific Knockout of RalGAPB Increases Glucose Disposal into BAT. We measured glucose uptake in mice after a 6-h fast. Glucose uptake into BAT was increased in ARGKO mice compared with control mice; in contrast, glucose uptake in gastrocnemius muscle and heart was reduced as compared with control mice. Glucose uptake into iWAT and epididymal WAT (eWAT) was moderately reduced, although not statistically significantly from controls (Fig. 2*B* and *SI Appendix*, Fig. S5*A*). Insulin levels were reduced during the experiment, with a trend toward reduced blood glucose levels, which may explain, in part, lower glucose uptake in insulin-responsive tissues other than BAT (Fig. 2 *C* and *D*). Additionally, Glut4 protein levels in gastrocnemius muscle were reduced, accompanied by a trend toward reduced Glut4 gene expression (*SI Appendix*, Fig. S5 *B–D*), although there were no differences in Glut1 or Glut4 levels in eWAT (*SI Appendix*, Fig. S5 *E* and *F*). In mature adipocytes isolated from eWAT, glucose uptake was increased twofold in the basal state and was reduced by 30% in insulin-stimulated conditions as compared with adipocytes from control mice (*SI Appendix*, Fig. S5*G*). These findings suggest that increased glucose disposal into BAT of ARGKO mice leads to reduced glucose uptake into other insulin-responsive tissues in order to maintain blood glucose levels within the physiological range, likely reflecting both lower insulin levels and Glut4 levels in muscle.

RalA Activation Increases Plasma Membrane Glut4 in Brown Fat. There was no change in protein levels of the glucose transporters Glut1 and Glut4 in BAT of ARGKO mice (*SI Appendix*, Fig. S6 *A* and *B*). The plasma membrane fraction derived from ARGKO mouse BAT contained more Glut4 and IRAP (known to colocalize with Glut4 in subcellular fractions) compared with control (Fig. 2 *E* and *F*). Mass spectrometry of plasma membrane fractions revealed that BAT plasma membranes from ARGKO mice contained seven times more Glut4 as compared with control (*SI Appendix*, Fig. S6 *C* and *D*), indicating that RalA regulates Glut4 recycling in BAT.

ARGKO Mice Exhibit Improved Glucose Handling. Body weight and food consumption were not changed in ARKGO mice on a normal diet (Fig. 3*A* and *SI Appendix*, Fig. S7*A*). ARGKO mice displayed improved glucose tolerance (11.5% decrease in area under the curve), accompanied by reduced insulin levels during the glucose tolerance test, and improved insulin tolerance as compared with control (Fig. 3 *B–E*). Blood glucose levels dropped faster in ARGKO mice upon food withdrawal, accompanied by a trend toward lower insulin levels (*SI Appendix*, Fig. S7 *B* and *C*). Blood glucose and insulin levels in the food-withdrawal experiment or during the glucose tolerance test were not elevated by RBC8 in ARGKO mice but were elevated in control mice (*SI Appendix*, Fig. S7 *D–F*). This is consistent with the observation that RBC8 does not inhibit RalA in ARGKO mice and strongly suggests that the RBC8-mediated increase in blood glucose levels is RalA dependent.

There was no difference in AKT phosphorylation between the genotypes before or after insulin injection in WAT, muscle, or liver, but insulin-stimulated AKT phosphorylation was reduced in BAT from ARGKO mice (*SI Appendix*, Fig. S8).

ARGKO Mice Exhibit Increased Nutrient Partitioning into Fat Depots. Even though the body weights and food intake of control and ARGKO mice were similar, ARGKO mice had a 35% increase in adiposity and a 1.35% decrease in lean mass as measured by NMR (Fig. 3 *F* and *G*). Tissue mass of all fat depots was increased in ARGKO mice compared with control mice, but the increase was most dramatic in BAT (Fig. 3*H*). H&E staining revealed that the expansion of fat depots was accompanied by increased cell size due to lipid accumulation. Median adipocyte size was increased 66% in iWAT and 24% in eWAT, although the latter effect did not reach statistical significance. H&E

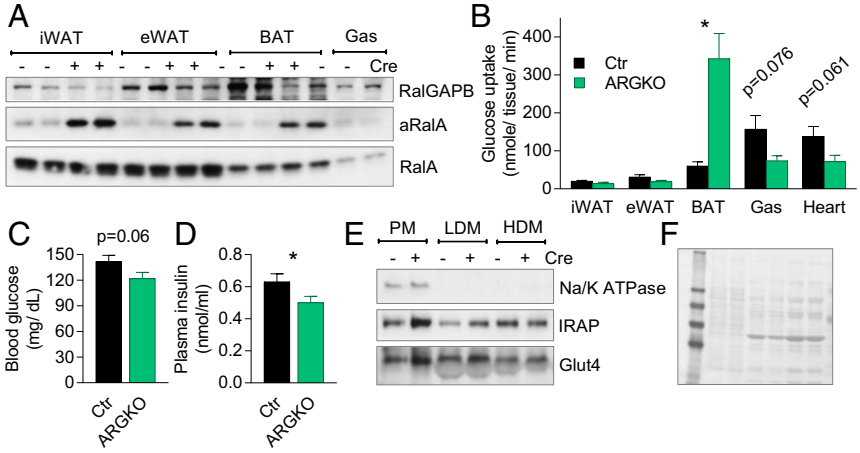

Fig. 2. RalGAPB knockout dramatically activates glucose uptake into BAT. Blood and tissues were collected from 8-wk-old mice after 6-h fast unless indicated otherwise. (*A*) WB of lysates from indicated tissues. Active RalA (aRalA) was determined by pull-down with RalBP1 agarose. (*B–D*) In vivo tissue-specific 2-deoxy-D-glucose uptake. Blood glucose (*C*) and insulin (*D*) levels before the experiment; eight mice per group. (*E* and *F*) Representative WB (out of five experiments) (*E*) and Ponceau stain (*F*) of BAT subcellular fractions collected after an overnight fast. The data are presented as mean ± SEM; $*P < 0.05$.

staining also revealed that brown adipocytes were larger, with larger lipid droplets. However, there was no increase in the number of small adipocytes typically associated with adipogenesis based on H&E staining and its quantitation (Fig. 3 *I–K*).

Previous studies have revealed a correlation of glucose uptake with the expression of de novo lipogenesis (DNL) genes and DNL itself in adipose tissue (14). Accordingly, expression of DNL genes was reduced in white fat depots and was increased in BAT of ARGKO mice (Fig. 3 *L* and *M* and *SI Appendix*, Fig. S9*A*). DNL was not affected in iWAT, eWAT, or liver but was increased in BAT, indicating that increased DNL in BAT is responsible for increased adiposity of ARGKO mice compared with control (Fig. 3*N* and *SI Appendix*, Fig. S9*B*).

ARGKO Mice Display Improved Glycemic Control on High-Fat Diet (HFD). Since we observed improved glucose handling and reduced insulin levels, we speculated that ARGKO mice may be protected from the development of metabolic disease during nutritional overload. Feeding mice a 45% fat diet for up to 20 wk produced no significant difference in weight gain between the genotypes (Fig. 4*A*). However, compared with control mice, ARGKO mice displayed a dramatic delay in the development of glucose and insulin intolerance during HFD feeding and displayed lower blood and insulin levels during fasting (Fig. 4 *B–F* and *SI Appendix*, Fig. S10).

Increased Glucose Disposal into BAT Drives Improved Glucose Handling. To explore the underlying mechanism of improved glucose handling and nutrient partitioning into fat depots on HFD, we measured glucose uptake in fasting and hyperinsulinemic-euglycemic clamp conditions. After a 6-h fast, total body glucose disposal was increased in ARGKO mice (despite a trend toward reduced insulin levels), explaining the reduction in fasting blood glucose (Fig. 4 *G–K*). Glucose uptake into BAT was dramatically increased in ARGKO mice on HFD, but to a lesser extent than that observed on normal diet. Glucose uptake into iWAT, gastrocnemius muscle, and heart was significantly decreased. Glucose uptake into eWAT was not affected (Fig. 4*L* and *SI Appendix*, Fig. S11*A*). The observed decreases in glucose uptake cannot be fully explained by reduced plasma insulin (*SI Appendix*, Fig. S11*B*) but may be partially explained by dramatically reduced blood glucose levels (*SI Appendix*, Fig. S11*C*).

Under hyperinsulinemic-euglycemic clamp conditions, there were no differences between control and ARGKO mice in glucose infusion rate, liver glucose production, or whole-body glucose disposal (Fig. 4 *M–P* and *SI Appendix*, Fig. S12 *A–C*). Analysis of tissue-specific glucose uptake revealed that glucose uptake into BAT was maximally activated in ARGKO mice under fasting conditions to an extent observed in insulin-stimulated wild-type mice, and was even further activated by insulin. However, the fold increase in glucose uptake into BAT of ARGKO mice was less dramatic under the clamp conditions (1.6-fold) than after a 6-h fast (3.4-fold). There was also no difference in glucose uptake in other insulin-responsive tissues during the clamp (Fig. 4*L* and *SI Appendix*, Fig. S12*D*). These data suggest that constitutive activation of RalA in adipose tissue mostly affects glucose homeostasis in the fasted state and works primarily by reducing insulin levels and improving glucose handling. It is somewhat surprising that improved glucose handling and lower insulin did not protect ARGKO mice from the development of peripheral insulin resistance. This may be explained by the observation that glucose uptake in BAT was inversely proportional to body weight and contributes less to metabolism in heavier, more insulin-resistant mice (*SI Appendix*, Fig. S12*E*).

Energy Expenditure Is Not Involved in Improving Metabolic Parameters in ARGKO Mice. Similar body weights and food intake between the genotypes indicate that ARGKO mice exhibit a redistribution of energy into adipose tissue without an overall change in energy balance. To that end, we observed that UCP1 expression in BAT from ARGKO mice was reduced compared with control mice on both normal diet and HFD. Expression of other thermogenic

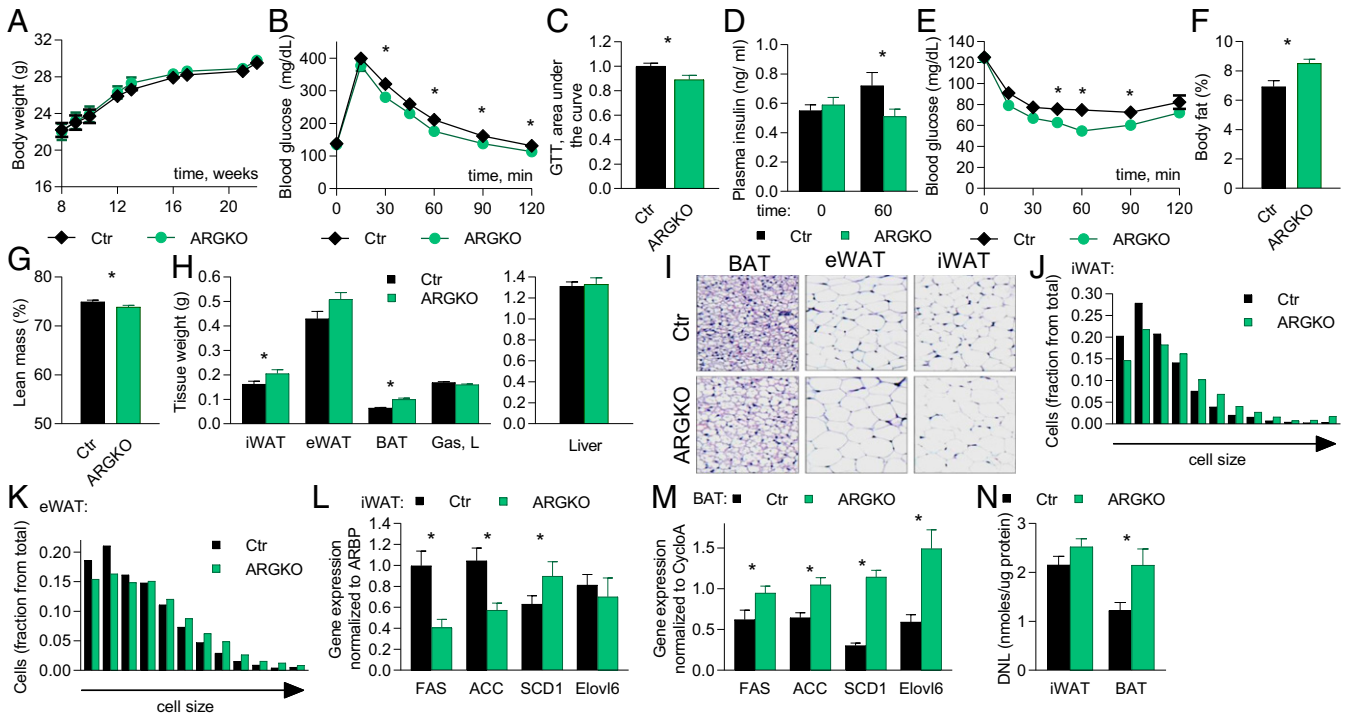

Fig. 3. ARGKO mice display increased nutrient partitioning into fat depots; 12 mice per group unless indicated otherwise. (*A*) Body weight. (*B–G*) The experiments are performed in 8-wk-old mice. (*B* and *C*) Glucose tolerance test (GTT) after 6-h fast (*B*) and area under the curve (*C*). (*D*) Insulin levels before and during GTT. (*E*) Insulin tolerance test after 3-h fast. (*F* and *G*) Body fat (*F*) and lean mass (*G*) measured by NMR. (*H–M*) The experiments were performed after 6-h fast in 23-wk-old mice. (*H*) Tissue weights. (*I–K*) H&E staining and quantitation of cell size of indicated fat depots; 10 images per group. (*L* and *M*) qPCR from iWAT (*L*) and BAT (*M*). (*N*) DNL in indicated tissues; six mice per group. The data are presented as mean ± SEM; $*P < 0.05$.

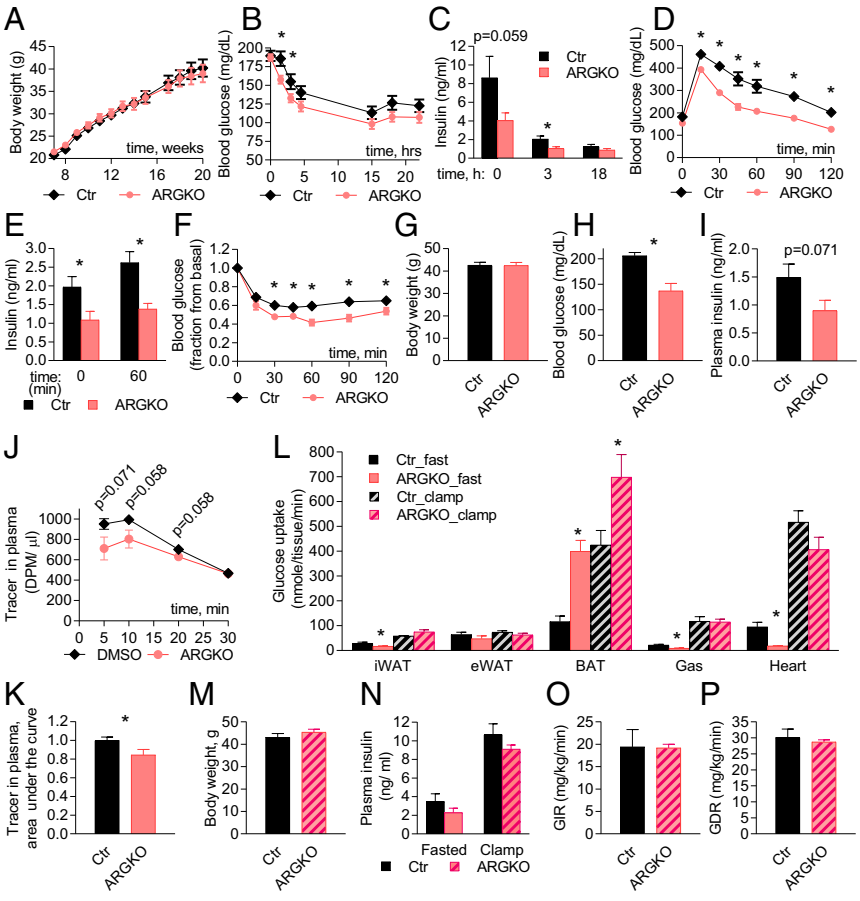

Fig. 4. Glucose handling is improved in ARGKO mice on HFD. Experiments were performed in 16-wk-old mice that have been on HFD for 8 wk; 12 mice per group were used unless indicated otherwise. (*A*) Body weight. (*B–F*) (*B* and *C*) Blood glucose (*B*) and insulin (*C*) after food withdrawal. (*D*) Glucose tolerance test (GTT) after 6-h fast. (*E*) Insulin levels before and during GTT. (*F*) Insulin tolerance test after 3-h fast. (*G–P*) Eight animals per group were used. (*G–K*) Biological parameters during 2-deoxy-D-glucose uptake experiment performed after 6-h fast. (*G*) Body weight. (*H*) Blood glucose. (*I*) Plasma insulin. (*J* and *K*) Radioactive glucose tracer decay in plasma (*J*) and area under the curve (*K*). (*L*) Tissue-specific glucose uptake measured in 6-h fasted animals or during the clamp. (*M–P*) Biological parameters during hyperinsulinemic-euglycemic clamp. (*M*) Body weight. (*N*) Plasma insulin. (*O*) Glucose infusion rate. (*P*) Glucose disposal rate. The data are presented as mean ± SEM; $*P < 0.05$.

genes were also reduced in BAT from ARGKO mice compared with control on normal diet, although expression of these genes was similar in control and ARGKO mice on HFD. This indicates that increased glucose uptake did not activate the thermogenic program in BAT (*SI Appendix*, Fig. S13).

Discussion

Previous studies have implicated RalA in the control of Glut4 recycling in 3T3-L1 adipocytes (6, 7, 9). We sought to investigate how the G protein might impact Glut4 exocytosis and glucose uptake in adipose tissue in vivo. We demonstrated that recently developed Ral inhibitors blocked glucose uptake in 3T3-L1 adipocytes, in primary adipocytes differentiated from iWAT and BAT, and in BAT in vivo. Moreover, adipocyte-specific knockout of the RalGAP complex in mice resulted in full activation of RalA in white and brown fat depots and was accompanied by increased glucose uptake into BAT in the basal state and by increased plasma membrane localization of Glut4. We also demonstrated that RalA is activated by feeding in BAT. Because RalGAP activity is repressed by insulin action via phosphorylation by AKT, causing activation of RalA, these data are consistent with a primary role for RalA in controlling insulin-stimulated glucose uptake. Importantly, these data establish that the RalGAP complex is a critical regulator of RalA activity and, more importantly, that RalA is a potent regulator of glucose uptake and cycling of the glucose transporter Glut4 in adipose tissue in vivo.

Although RalA inhibitors reduced insulin-stimulated glucose uptake in both white and brown adipocytes differentiated from stromal vascular fraction, we were surprised to note that activation of RalA by RalGAPB knockout had differential effects on glucose uptake in the different fat depots in vivo. While RalA activation dramatically facilitated glucose uptake in BAT in the basal state, glucose uptake into iWAT was reduced (together with a reduction into gastrocnemius muscle and heart). Although the reasons for these differences remain uncertain, there are several possible explanations. It is possible that other signals are required in white adipocytes for the full expression of insulin's actions on Glut4 that are less important in brown fat. It is also likely that reduced in vivo glucose disposal in WAT and muscle in ARGKO mice may reflect a compensatory mechanism to maintain glucose levels in a narrow range. This reduced in vivo glucose disposal is also reflected by lower circulating insulin levels as well as lower Glut4 protein levels in muscle from mice on normal diet. Supporting this hypothesis, basal glucose uptake was twofold higher in mature adipocytes isolated from eWAT of ARGKO mice. Moreover, despite decreased in vivo glucose uptake and reduced expression of DNL genes, iWAT was expanded in ARGKO mice. One possible explanation is that BAT in ARGKO mice clears less lipid from the circulation as compared with control mice and that these lipids are incorporated into WAT, leading to increased adipocyte size. This hypothesis will need to be experimentally addressed.

Brown fat and heart have the highest glucose uptake rate per gram of tissue. Cold exposure substantially increases glucose uptake in BAT and, thus, may be responsible for disposal of up to three-fourths of ingested glucose in mice (15, 16). In human subjects with measurable BAT, cold exposure significantly increases whole-body glucose disposal and insulin sensitivity as compared with subjects without BAT (17). In addition, an increase in the amount of BAT positively impacts whole-body metabolism, even in the absence of cold exposure. For example, BAT transplants improve glucose tolerance and insulin sensitivity and lead to weight loss in mice (18). The effect of increasing glucose uptake in BAT without a corresponding increase in thermogenesis on whole-body glucose homeostasis has not been examined. RalA activation dramatically increased glucose uptake into BAT and had profound effects on whole-body glucose and lipid metabolism.

ARGKO mice displayed improved glucose handling, lower insulin levels, and increased adiposity. It is likely that there are several factors contributing to this overall improvement in metabolic health. First, the constitutive translocation of glucose transporters to the plasma membrane in ARGKO BAT produced a profound repartitioning of energy into this tissue, which was accompanied by enhanced DNL to accommodate increased glucose uptake. Second, the increased glucose uptake in BAT also lowered circulating insulin levels, which contributed to reduced glucose uptake in muscle and WAT. Thus, this study demonstrates that increased glucose uptake into BAT, without activation of energy expenditure, influences whole-body glucose homeostasis in a positive way. Therefore, targeting glucose uptake in BAT via inhibition of RalGAP might provide beneficial effects on whole-body glucose homeostasis.

Methods

Treatment of 3T3-L1 Adipocytes with Ral Inhibitors. 3T3-L1 adipocytes were serum starved overnight in DMEM with 0.5% FBS and then pretreated with Ral inhibitors or DMSO for 1 h in Krebs-Ringer Hepes buffer (120 mM NaCl, 4.8 mM KCl, 1.3 mM $CaCl_2$, 1.2 mM KH_2PO_4, 1.2 mM $MgSO_4$, and 20 mM Hepes, pH 7.4). BQU57 was routinely used at 100 μM, and RBC8 at 50 μM. Next, the cells were stimulated with 10 nM insulin for an additional 30 min in the presence of the inhibitors and were either used to extract proteins for Western blotting (WB), fixed for imaging, or used to measure glucose uptake.

TIRF Microscopy. 3T3-L1 adipocytes constitutively expressing Myc7-Glut4-EGFP were pretreated with 100 nM BQU57 or DMSO for 1 h and then washed into phenol red-free DMEM (Invitrogen) supplemented with BQU57 or DMSO. Cells were imaged with a GE DeltaVision OMX microscope equipped with an Evolve 512 (Photometrics) camera, with 60× oil objective (n.a. 1.45) and DeltaVision OMX software. Excitation was performed with a 488 nm laser. During imaging, cells were enclosed in a 37 °C heated chamber with 5% CO_2. See *SI Appendix, Supplementary Methods* for image processing.

Glucose Uptake in 3T3-L1 Adipocytes. After pretreatment with Ral inhibitors and stimulation with insulin, 3T3-L1 adipocytes were incubated with 40 μM 2-deoxy-D-[H^3]-glucose (stock: H^3, 1 mCi/mL; specific activity 8.7 Ci/mmol) for 5 min. The uptake was terminated by addition of 15 μM cytocholasin B for 5 min. The cells were then washed with cold PBS to remove radioactivity and lysed in 0.1 M NaOH (200 μL). The lysate was neutralized with 0.1 M HCl (200 μL) and used for scintillation counting.

DNL in 3T3-L1 Adipocytes. After pretreatment with Ral inhibitors and stimulation with insulin, 3T3-L1 adipocytes were incubated with 40 μM C^{14}-labeled glucose for 30 min. The cells were then lysed in 200 μL of 1 N KOH and neutralized with 200 μL of 1 N HCl. To 200 μL of that lysate, 800 μL of chlorophorm–methanol (2:1) solution was added, and then the mixture was vortex-mixed, incubated for 5 min at room temperature, and centrifuged for 15 min at 10,000 × *g*. Next, 400 μL of the bottom fraction was moved to scintillation vials, completely dried overnight in a fume hood, resuspended in scintillation liquid, and counted.

Mouse Studies. Mice were housed in a specific pathogen-free facility with a 12-h light/12-h dark cycle, and given free access to food and water, except for fasting period. All animal use was approved by the Institutional Animal Care and Use Committees at the University of California, San Diego and the University of Michigan. See *SI Appendix, Supplementary Methods* for the description of RalGAPB knockout mice and for the diets used.

In Vivo RBC8 Treatment and Tissue-Specific Glucose Uptake. Ad libitum-fed C57BL/6J mice were i.p. injected with 50 mg/kg of RBC8 in DMSO or with DMSO alone. For glucose uptake measurement, 40 min after RBC8 injection, mice were i.p. injected with 10 μCi of deoxy-D-2-[14C(U)]-glucose and, 30 min later, the mice were killed and tissues were collected. See *SI Appendix, Supplementary Methods* for more information.

BAT Fractionation. BAT fractionation was performed as previously described for WAT (19). Briefly, BAT was dissected from overnight-fasted mice. Adipocytes were isolated by digestion with collagenase as described in *SI Appendix, Supplementary Methods*, and then washed, homogenized in sucrose buffer, and subjected to series of centrifugations in sucrose buffers to separate high-density microsomes, low-density microsomes, and plasma membrane, based on buoyancy. The pellets were resuspended in a lysis buffer buffer (*SI Appendix, Supplementary Methods*) and processed for WB, or resuspended in water and processed for mass spectrometry. See *SI Appendix, Supplementary Methods* for more information.

In Vivo DNL. Mice were i.p. injected with 0.035 mL (per gram of body weight) D2O in 0.9% NaCl and housed for 1 wk with drinking water containing 8% D2O. The water consumption was monitored. On day 7, the mice were fasted for 6 h, killed, and their tissues were collected, frozen in liquid nitrogen, and stored at −80 °C. For mass spectrometry, the tissues were processed as previously described (20, 21). See more in *SI Appendix, Supplementary Methods*.

Hyperinsulinemic-Euglycemic Clamp. Male C57BL/6J mice received a 45% HFD for 8 wk. Mouse clamps were performed as described previously (22). See *SI Appendix, Supplementary Methods* for more information.

Statistical Analyses. Two-tailed *t* tests were used for comparison between two groups. All comparisons were two-sided, and *P* values of less than 0.05 were considered to indicate statistical significance. Averaged values are presented as the mean ± SEM.

ACKNOWLEDGMENTS. We thank the Metabolomics Core at the University of Michigan for performing NMR measurements of body composition; the Histology Core at the University of Michigan School of Dentistry; the Histology Core at Moores Cancer Center at the University of California, San Diego; and the Biomolecular and Proteomics Mass Spectrometry Facility at the University of California, San Diego. This work was supported by NIH Grants DK076906, DK061618, and DK060591 (to A.R.S.); P30 DK063491, 16POST27740033 (to Y.S.); and ADA 1-18-PDF-094 (to C.-W.H).

1. Rosen ED, Spiegelman BM (2006) Adipocytes as regulators of energy balance and glucose homeostasis. *Nature* 444:847–853.
2. Kershaw EE, Flier JS (2004) Adipose tissue as an endocrine organ. *J Clin Endocrinol Metab* 89:2548–2556.
3. Shepherd PR, et al. (1993) Adipose cell hyperplasia and enhanced glucose disposal in transgenic mice overexpressing GLUT4 selectively in adipose tissue. *J Biol Chem* 268: 22243–22246.
4. Morley TS, Xia JY, Scherer PE (2015) Selective enhancement of insulin sensitivity in the mature adipocyte is sufficient for systemic metabolic improvements. *Nat Commun* 6:7906.
5. Leto D, Saltiel AR (2012) Regulation of glucose transport by insulin: Traffic control of GLUT4. *Nat Rev Mol Cell Biol* 13:383–396.
6. Chen XW, Leto D, Chiang SH, Wang Q, Saltiel AR (2007) Activation of RalA is required for insulin-stimulated Glut4 trafficking to the plasma membrane via the exocyst and the motor protein Myo1c. *Dev Cell* 13:391–404.
7. Chen XW, et al. (2011) A Ral GAP complex links PI 3-kinase/Akt signaling to RalA activation in insulin action. *Mol Biol Cell* 22:141–152.
8. Leto D, Uhm M, Williams A, Chen XW, Saltiel AR (2013) Negative regulation of the RalGAP complex by 14-3-3. *J Biol Chem* 288:9272–9283.
9. Chen XW, et al. (2011) Exocyst function is regulated by effector phosphorylation. *Nat Cell Biol* 13:580–588.
10. Yan C, et al. (2014) Discovery and characterization of small molecules that target the GTPase Ral. *Nature* 515:443–447.
11. Huang S, et al. (2007) Insulin stimulates membrane fusion and GLUT4 accumulation in clathrin coats on adipocyte plasma membranes. *Mol Cell Biol* 27:3456–3469.
12. Lizunov VA, Stenkula K, Troy A, Cushman SW, Zimmerberg J (2013) Insulin regulates Glut4 confinement in plasma membrane clusters in adipose cells. *PLoS One* 8:e57559.
13. Lizunov VA, Matsumoto H, Zimmerberg J, Cushman SW, Frolov VA (2005) Insulin stimulates the halting, tethering, and fusion of mobile GLUT4 vesicles in rat adipose cells. *J Cell Biol* 169:481–489.
14. Herman MA, et al. (2012) A novel ChREBP isoform in adipose tissue regulates systemic glucose metabolism. *Nature* 484:333–338.
15. Orava J, et al. (2011) Different metabolic responses of human brown adipose tissue to activation by cold and insulin. *Cell Metab* 14:272–279.
16. Bartelt A, et al. (2011) Brown adipose tissue activity controls triglyceride clearance. *Nat Med* 17:200–205.
17. Chondronikola M, et al. (2014) Brown adipose tissue improves whole-body glucose homeostasis and insulin sensitivity in humans. *Diabetes* 63:4089–4099.
18. Stanford KI, et al. (2013) Brown adipose tissue regulates glucose homeostasis and insulin sensitivity. *J Clin Invest* 123:215–223.
19. Simpson IA, et al. (1983) Insulin-stimulated translocation of glucose transporters in the isolated rat adipose cells: Characterization of subcellular fractions. *Biochim Biophys Acta* 763:393–407.
20. Zhao S, et al. (2016) ATP-citrate lyase controls a glucose-to-acetate metabolic switch. *Cell Rep* 17:1037–1052.
21. Svensson RU, et al. (2016) Inhibition of acetyl-CoA carboxylase suppresses fatty acid synthesis and tumor growth of non-small-cell lung cancer in preclinical models. *Nat Med* 22:1108–1119.
22. Hevener AL, et al. (2003) Muscle-specific Pparg deletion causes insulin resistance. *Nat Med* 9:1491–1497.